IEEE Access
Multidisciplinary | Rapid Review | Open Access Journal

Received June 20, 2019, accepted June 27, 2019, date of publication July 2, 2019, date of current version July 22, 2019.

Digital Object Identifier 10.1109/ACCESS.2019.2926361

Stability Analysis and Oscillation Mechanism of the DFIG-Based Wind Power System

WEI JIN AND YUPING LU, (Senior Member, IEEE)
School of Electrical Engineering, Southeast University, Nanjing 210096, China

Corresponding author: Wei Jin (230159510@seu.edu.cn)

This work was supported in part by the National Natural Science Foundation of China under Grant 51677026.

ABSTRACT The interaction between the DFIG (doubly fed induction generator)-based wind farm and the ac grid makes the traditional positive-sequence subsystem and negative-sequence subsystem no longer decoupled, so the single-input single-out (SISO) characteristic in the frequency domain no longer holds. In this paper, the admittance models of the DFIG and ac grid are established by using the small-signal analysis method. On this basis, first the admittance relationship of the entire DFIG-based wind power system in polar coordinates is obtained. Second, the multi-input multi-output (MIMO) system is simplified into an SISO system by the matrix transformation. Then, the characteristic equation and the equivalent circuit of the DFIG-based wind power system are provided. In cases of a weak ac grid, low wind speed and a high proportional coefficient of the phase-locked loop (PLL) controller, the stability of the DFIG-based wind power system will be weakened, and the oscillation among different coupling frequencies will occur based on Nyquist criterion. Finally, the simulation results show the correctness of the theoretical analysis.

INDEX TERMS DFIG-based wind power system, stability analysis, Nyquist criterion, frequency-coupling PLL, grid strength, wind speed.

I. INTRODUCTION

New sources of low-carbon, clean and sustainable energy have received widespread attention worldwide. With the continuous expansion of new energy connected to systems, especially for large-scale wind power connected to the AC grid, the impact of the new energy makes power systems become increasingly difficult to ignore [1]– [5].

As the most suitable new energy for large-scale development and utilization, wind power has clearly changed the dynamic characteristics of the power system [6]– [8]. However, the wind power has its own typical characteristics. First, wind farms usually cover a relatively wide area, and the wind power connects to the AC grid through long-distance outgoing lines, so that the AC grid strength decreases with the increasing length of the outgoing line. Second, the wind turbine generates electricity by wind, and the dynamic characteristics of the wind turbine are related to the wind speed. However, the wind speed is uncontrollable and related to the weather. In addition, the wind generator is synchronized with the AC grid through the PLL [9]. However, the dynamic characteristics of the PLL are related to its own controller parameters, which affect the wind power system. All of these characteristics make the interaction between wind farm and AC grid more complicated, which introduces the stability and oscillation problem of the wind power system, posing a threat to the security of the power system.

In recent years, the impedance-based method [10]– [17] has been widely used in analyzing the stability and oscillation mechanism of the new energy grid-connected system. Generally, modeling-based methods in the *dq* coordinate system [11], [12] or *xy* stationary coordinate system [13]– [16] are used. In [10] and [11], the impedance modeling-based method in the *dq* coordinate system is studied. In [12], the relationship between the impedance model in the *dq*coordinate system and the static coordinate system is revealed. Furthermore, a unified impedance model of grid-connected inverters is established in the static coordinate system. A modeling method of harmonic linearization in the frequency domain is proposed in [13]– [15]. In [16], [17], the impedance model of grid-connected inverters is derived considering the frequency-coupling characteristics. The applied precondition of these methods is to decouple the positive and negative sequence components. However,

The associate editor coordinating the review of this manuscript and approving it for publication was Giambattista Gruosso.

the d-axis and q-axis are asymmetrical when wind generators connect to the AC grid through the PLL, which results in a coupling relationship between different frequencies.

At present, some scholars have conducted fruitful research on the DFIG-based wind power system [18]– [26]. In [18]– [21], the DFIG impedance model is established considering the rotor-side converter (RSC) and grid-side converter (GSC). The GSC controller has little influence on the DFIG impedance and can be ignored. Furthermore, the effect of the wind speed, controller parameters and series compensation on the DFIG-based wind power system is analyzed in detail. In [22] and [23], the DFIG impedance model in the stationary coordinate system is preliminarily established considering the PLL. In [24]– [26], the dynamic characteristics of the PLL and current loop greatly affect the system stability in wind power systems. Previous works are undoubtedly very meaningful. However, the equivalent circuit of the wind power system is not clear, so accurate, effective and simple methods should be further investigated.

The wind power system is essentially an MIMO system. To more accurately study the dynamic characteristics of the wind power system, the RSC and GSC controller of the DFIG are first modeled in detail. Then, the equivalent admittance model of the DFIG is obtained. A unified admittance model of the DFIG-based wind farm connected to the AC grid considering the PLL, rotor speed and grid strength is established. By splitting the admittance matrix and transforming coordinates, the characteristic equation of the wind power system is obtained. Meanwhile, the coupling circuit between the equivalent positive-sequence and negative-sequence in the polar coordinate system is obtained. Furthermore, based on Nyquist criterion, the effect of the PLL, wind speed and grid strength on the stability of the DFIG-based wind power system is analyzed. In the case of wind power system oscillation due to loss of stability, the frequency coupling phenomenon is verified by simulation.

II. DFIG-BASED WIND POWER SYSTEM

When the operating conditions of various wind turbines in the wind farm are not notably different, the entire wind farm can be replaced by a DFIG [27], [28]. Therefore, the equivalent wind power system is shown in Figure 1.

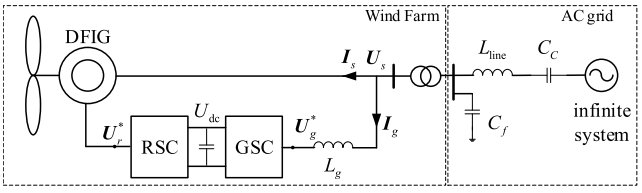

FIGURE 1. DFIG-based wind farm connected to the AC grid.

where $\boldsymbol{U}$ and $\boldsymbol{I}$ are the voltage and current of the DFIG, respectively, R is the resistance, L is the inductance, and L_m is the magnetizing inductance. The subscripts s, r and g are the stator, rotor and grid side, respectively; d and q are the d-axis and q-axis components, respectively. C_f is the capacitance of SVC. L_{line} and C_C are the equivalent inductance and capacitance of the series-compensated transmission line, respectively. In addition, ω_1 and ω_2 are the synchronous angular frequency and rotor frequency component, respectively. Thus, $\omega_2 = \sigma_{slip}\omega_1$, where σ_{slip} is the slip of the DFIG.

For convenience, the dynamic models between different coordinate systems are first established. The relationship between the system reference coordinate system (xy coordinate system) and the controller reference coordinate system (dq coordinate system) is shown in Figure 2 [29].

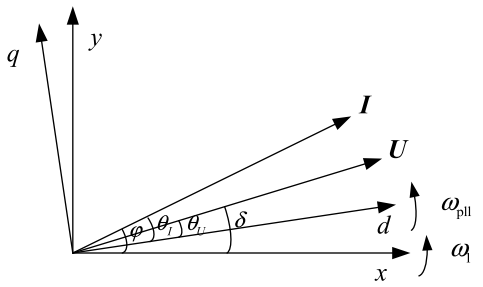

FIGURE 2. Rotation vectors in different coordinate systems under disturbance.

The xy coordinate system is the global coordinate system that rotates at synchronous speed ω_1, whereas the dq coordinate system is the controller coordinate system that rotates at speed ω_{pll} measured by the PLL. The angle between the two coordinate systems is θ_{pll}. θ_I and θ_U are the phase angles of the current and voltage in the controller coordinate system (dq coordinate system), respectively, while φ and δ are the phase angles of the current and voltage in the system reference coordinate system (xy coordinate system), respectively.

Obviously, we have

$$\begin{cases} \theta_U = \delta - \theta_{\text{pll}} \\ \theta_I = \varphi - \theta_{\text{pll}} \end{cases} \tag{1}$$

The control block diagram of the synchronous rotating coordinate system PLL is shown in Figure 3 [22], [30].

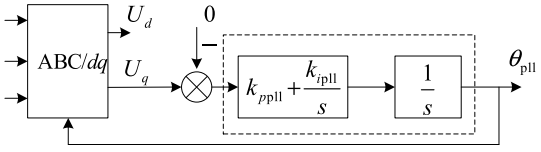

FIGURE 3. Control block diagram of PLL.

As shown in Figure 3, the relationship between the q-axis voltage U_q and the PLL output angle θ_{pll} is given by

$$\begin{cases} \theta_{\text{pll}} = G_{\text{pll}}(s)U_q \\ \omega = s\theta_{\text{pll}} + \omega_0 \end{cases} \tag{2}$$

where $G_{pll} = \frac{1}{s}(k_{p\text{pll}} + \frac{k_{i\text{pll}}}{s})$.

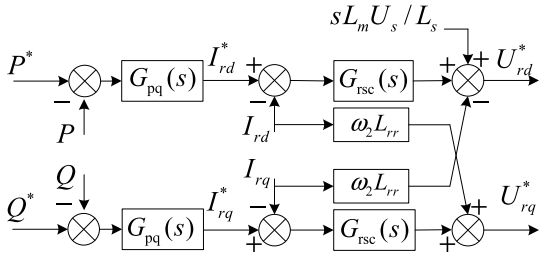

FIGURE 4. Control block diagram of RSC.

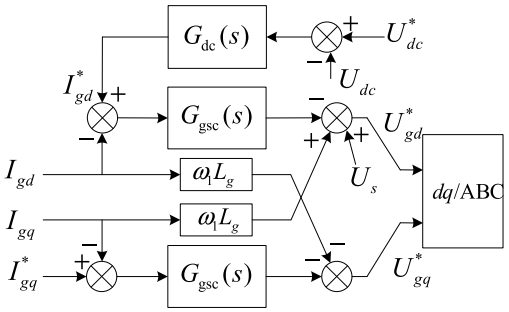

FIGURE 5. Control block diagram of GSC.

The RSC and GSC control block of DFIG in the dq coordinate system are shown in Figure 4 and Figure 5, respectively [31]– [34].

where $L_s = L_m + L_{\sigma s}, L_r = L_m + L_{\sigma r}$ and $L_{rr} = L_s - L_m^2/L_r$.

According to the control block diagram of RSC and GSC, the relationship between the voltage and current components in thedq coordinate system can be written as shown in (3) and (4).

$$\begin{cases} U^*_{rd} = G_{\rm rsc}(s)(I^*_{rd} - I_{rd}) - \omega_2 L_{rr} I_{rq} + \dfrac{\sigma_{slip} L_m U_s}{L_s} \\ U^*_{rq} = G_{\rm rsc}(s)(I^*_{rq} - I_{rq}) + \omega_2 L_{rr} I_{rd} \end{cases} \tag{3}$$

$$\begin{cases} U^*_{gd} = G_{\rm gsc}(s)(I^*_{gd} - I_{gd}) - \omega_1 L_g I_{gq} + U_s \\ U^*_{gq} = G_{\rm gsc}(s)(I^*_{gq} - I_{gq}) + \omega_1 L_g I_{gd} \end{cases} \tag{4}$$

where $G_{\rm rsc}(s) = K_{p\rm rsc} + \frac{K_{i\rm rsc}}{s}$, and $G_{\rm gsc}(s) = K_{p\rm gsc} + \frac{K_{i\rm gsc}}{s}$.

III. ADMITTANCE MODEL OF DFIG-BASED WIND POWER SYSTEM

In this paper, the following conditions are assumed: the output power factor of DFIG is close to 1, and the AC grid is stable.

Due to the multi-time scale characteristics of the DFIG converter control system, the response of the outer loop is slower than that of the inner loop. Therefore, we divide the DFIG converter control system into two processes. First, only the dynamic of the inner loop is considered. Then, the dynamic of the outer loop is considered.

A. ADMITTANCE MODELING OF THE DFIG REGARDLESS OF THE OUTER LOOP CONTROL

In the dq coordinate system, the stator and rotor voltage equations of the DFIG are written as shown in (5) and (6), respectively.

$$\begin{cases} U_{sd} = (R_s + sL_s) I_{sd} + sL_m I_{rd} - \omega_1 L_s I_{sq} - \omega_1 L_m I_{rq} \\ U_{sq} = (R_s + sL_s) I_{sq} + sL_m I_{rq} + \omega_1 L_s I_{sd} + \omega_1 L_m I_{rd} \end{cases} \tag{5}$$

$$\begin{cases} U_{rd} = (R_r + sL_r) I_{rd} + sL_m I_{sd} - \omega_2 L_r I_{rq} - \omega_1 L_m I_{sq} \\ U_{rq} = (R_r + sL_r) I_{rq} + sL_m I_{sq} + \omega_2 L_r I_{rd} + \omega_1 L_m I_{sd} \end{cases} \tag{6}$$

Similarly, the GSC voltage equation of the DFIG is

$$\begin{cases} U_{sd} = (R_g + sL_g) I_{gd} - \omega_1 L_g I_{gd} + U^*_{gd} \\ U_{sq} = (R_g + sL_g) I_{gq} + \omega_1 L_g I_{gq} + U^*_{gq} \end{cases} \tag{7}$$

We transform those equations into the polar coordinate system corresponding to the xy coordinate system. Substituting (1)-(3) into (5) and (6) yields the simultaneous solutions in (8) (The derivation process is shown in Appendix A):

$$\begin{bmatrix} \Delta I_s \\ I_s \Delta\varphi \end{bmatrix} = \begin{bmatrix} Y_{s1} & Y_{s2} \\ Y_{s3} & Y_{r4} \end{bmatrix} \begin{bmatrix} \Delta U_s \\ U_s \Delta\delta \end{bmatrix} \tag{8}$$

Equation (8) is the approximate dynamic model between the stator side voltage and the current of the DFIG, where

$$\begin{cases} Y_{s1} = \dfrac{1}{\frac{R_r}{\sigma_{slip}} + sL_{\sigma s} + sL_{\sigma r} - \frac{1}{\sigma_{slip}} G_{\rm rsc}(s)} \\ Y_{s2} = 0 \\ Y_{s3} = 0 \\ Y_{s4} = \dfrac{1}{(1 + G_{\rm pll}(s) U_s)(\frac{R_r}{\sigma_{slip}} + sL_{\sigma s} + sL_{\sigma r} - \frac{1}{\sigma_{slip}} G_{\rm rsc}(s))}. \end{cases}$$

Similarly, substituting (1), (2) and (4) into (7) yields the simultaneous solutions in (9) (the derivation process is shown in Appendix A):

$$\begin{bmatrix} \Delta I_g \\ I_g \Delta\varphi \end{bmatrix} = \begin{bmatrix} Y_{g1} & Y_{g2} \\ Y_{g3} & Y_{g4} \end{bmatrix} \begin{bmatrix} \Delta U_s \\ U_s \Delta\delta \end{bmatrix} \tag{9}$$

Equation (9) is the approximate dynamic model between the grid side voltage and the current of the DFIG.

$$\text{where} \begin{cases} Y_{g1} = \dfrac{1}{sL_g - G_{\rm gsc}(s)} \\ Y_{g2} = 0 \\ Y_{g3} = 0 \\ Y_{g4} = \dfrac{1}{(1 + G_{\rm pll}(s) U_s)(sL_g - G_{\rm gsc}(s))}. \end{cases}$$

The modulus of $G_{\rm pll}(s)$ decreases with the increase in frequency, which makes Y_{s1} tend to Y_{s4} and Y_{g1} tend to Y_{g4}. In particular, when the frequency is sufficiently high, there are $Y_{s1} \approx Y_{s4}$ and $Y_{g1} \approx Y_{g4}$.

B. ADMITTANCE MODELING OF THE DFIG CONSIDERING THE OUTER LOOP CONTROL

When the dynamic of low-frequency signal must be considered, the effect of the outer loop controller on the system stability cannot be ignored. The outer control block diagrams of GSC and RSC are shown in Figures 4 and 5.

1) CONSIDERING THE PQ CONTROL OF THE RSC

When considering the PQ control, the following dynamic equations of the outer loop controller in (10) and (11) should be included into the rotor side dynamic equations.

$$\begin{cases} I_{rd}^* = (P_s^* - P_s)G_{\mathrm{pq}}(s) \\ I_{rq}^* = (Q_s^* - Q_s)G_{\mathrm{pq}}(s) \end{cases} \tag{10}$$

$$\begin{cases} P_s = U_{sd}I_{sd} + U_{sq}I_{sq} \\ Q_s = -U_{sd}I_{sq} + U_{sq}I_{sd} \end{cases} \tag{11}$$

where $G_{\mathrm{pq}}(s)$ is the transfer function of the power outer loop controller. P_s^* and Q_s^* are the reference values of active and reactive power, respectively.

By linearizing (10) and (11) and substituting these equations into the stator voltage equations, the stator-side dynamic model in polar coordinates is expressed as shown in (12). (The detailed derivation is shown in Appendix A)

$$\begin{bmatrix} \Delta I_s \\ I_s\Delta\varphi \end{bmatrix} = \begin{bmatrix} Y_{s1} & Y_{s2} \\ Y_{s3} & Y_{r4} \end{bmatrix} \begin{bmatrix} \Delta U_s \\ U_s\Delta\delta \end{bmatrix} \tag{12}$$

where

$$\begin{cases} Y_{s1} = \dfrac{1}{sL_{\sigma s} + \frac{R_r}{\sigma_{slip}} + sL_{\sigma r} + G_{\mathrm{pq}}(s)G_{\mathrm{rsc}}(s)U_s - \frac{1}{\sigma_{slip}}G_{\mathrm{rsc}}(s)} \\ Y_{s2} = 0 \\ Y_{s3} = 0 \\ Y_{s4} = \dfrac{\frac{1}{1+G_{\mathrm{pll}}(s)U_s}}{sL_{\sigma s} + \frac{R_r}{\sigma_{slip}} + sL_{\sigma r} + G_{\mathrm{pq}}(s)G_{\mathrm{rsc}}(s)U_s - \frac{1}{\sigma_{slip}}G_{\mathrm{rsc}}(s)}. \end{cases}$$

2) CONSIDERING THE DC BUS VOLTAGE CONTROL

When considering the DC voltage control of the GSC, the DC voltage control equation and dynamic equation of the DC capacitance are given by

$$I_{gd}^* = (U_{\mathrm{dc}} - U_{\mathrm{dc}}^*)G_{\mathrm{dc}}(s) \tag{13}$$

$$U_{\mathrm{dc}}C_{\mathrm{dc}}\frac{\mathrm{d}U_{\mathrm{dc}}}{\mathrm{d}t} = -P_{\mathrm{e}} + P_{\mathrm{m}} \tag{14}$$

where U_{dc}^* and U_{dc} are the reference and actual values of the DC bus voltage, P_{m} is the actual input power of the DFIG (assumed constant), P_{e} is the output power of the DFIG, and $G_{\mathrm{dc}}(s)$ is the transfer function of the DC voltage controller.

Similarly, the grid side dynamic model of the DFIG can be written as shown in (15). (The detailed derivation is shown in Appendix A).

$$\begin{bmatrix} \Delta I_g \\ I_g\Delta\varphi \end{bmatrix} = \begin{bmatrix} Y_{g1} & Y_{g2} \\ Y_{g3} & Y_{g4} \end{bmatrix} \begin{bmatrix} \Delta U_s \\ U_s\Delta\delta \end{bmatrix} \tag{15}$$

where

$$\begin{cases} Y_{g1} = \dfrac{1 - \frac{G_{\mathrm{gsc}}(s)G_{\mathrm{dc}}(s)I_{s0}(\sigma_{slip}-1)}{\sigma_{slip}sU_{\mathrm{dc}0}C_{\mathrm{dc}}}}{sL_g - G_{\mathrm{gsc}}(s)(1 - \frac{G_{\mathrm{dc}}(s)U_{s0}(\sigma_{slip}-1)}{\sigma_{slip}sU_{\mathrm{dc}0}C_{\mathrm{dc}}})} \\ Y_{g2} = 0 \\ Y_{g3} = 0 \\ Y_{g4} = \dfrac{1}{(1 + G_{\mathrm{pll}}(s)U_s)(sL_g - G_{\mathrm{gsc}}(s))} \end{cases}$$

C. ADMITTANCE MODEL OF THE AC GRID

Assuming that the resistance, inductance and capacitance of the element are expressed by R, L and C, respectively, the impedance matrix of the resistance, inductance and capacitance can be written as follows in consideration of the component coupling.

$$\begin{cases} \boldsymbol{Z}_{\mathrm{R}} = \begin{bmatrix} R & 0 \\ 0 & R \end{bmatrix} \\ \boldsymbol{Z}_L = \begin{bmatrix} s & -\omega \\ \omega & s \end{bmatrix} L \\ \boldsymbol{Z}_{\mathrm{C}} = \dfrac{1}{\begin{bmatrix} s & -\omega \\ \omega & s \end{bmatrix} C} \end{cases} \tag{16}$$

It can be proven that the following equation remains valid: $\boldsymbol{Y}_R = \boldsymbol{Z}_R^{-1}$, $\boldsymbol{Y}_L = \boldsymbol{Z}_L^{-1}$, and $\boldsymbol{Y}_C = \boldsymbol{Z}_C^{-1}$.

In the xy coordinate system, by Ohm's law, the linearized dynamic equation of element k can be given by

$$\begin{bmatrix} \Delta I_{kx} \\ \Delta I_{ky} \end{bmatrix} = \boldsymbol{Y}_k\left(\begin{bmatrix} \Delta U_{ix} \\ \Delta U_{iy} \end{bmatrix} - \begin{bmatrix} \Delta U_{jx} \\ \Delta U_{jy} \end{bmatrix}\right) \tag{17}$$

where i and j are the node number at both ends of the element respectively, and k is the element number. $\boldsymbol{Y}_k$ is the admittance coupling matrix of element k.

Introducing ϕ_i as the power factor angle of the i-th node, equation (17) can be written as shown in (18) in the polar coordinate system.

$$\begin{bmatrix} \Delta I_k \\ I_k\Delta\varphi_k \end{bmatrix} = \boldsymbol{Y}_k\left(\begin{bmatrix} \cos\phi_i & -\sin\phi_i \\ \sin\phi_i & \cos\phi_i \end{bmatrix} \begin{bmatrix} \Delta U_i \\ U_i\Delta\delta_i \end{bmatrix} - \begin{bmatrix} \cos\phi_j & -\sin\phi_j \\ \sin\phi_j & \cos\phi_j \end{bmatrix} \begin{bmatrix} \Delta U_j \\ U_j\Delta\delta_j \end{bmatrix}\right) \tag{18}$$

The power factor of each node is approximately 1 when the wind power is sent [26]. Therefore, $\cos\phi \approx 1$ and $\sin\phi \approx 0$. The nodal voltage equation is formulated according to the grid structure as shown in Figure 1. (The inflow port current is positive)

$$\begin{bmatrix} \Delta\boldsymbol{I}_1 \\ \boldsymbol{0} \end{bmatrix} = \begin{bmatrix} \boldsymbol{Y}_{11} & -\boldsymbol{Y}_{12} \\ -\boldsymbol{Y}_{21} & \boldsymbol{Y}_{22} \end{bmatrix} \begin{bmatrix} \Delta\boldsymbol{U}_1 \\ \Delta\boldsymbol{U}_2 \end{bmatrix} \tag{19}$$

where

$$\begin{cases} \boldsymbol{Y}_{11} = \boldsymbol{Y}_{C_f} + \boldsymbol{Y}_{L_{\mathrm{line}}} \\ \boldsymbol{Y}_{12} = \boldsymbol{Y}_{21} = \boldsymbol{Y}_{L_{\mathrm{line}}} \\ \boldsymbol{Y}_{22} = \boldsymbol{Y}_{C_C} + \boldsymbol{Y}_{L_{\mathrm{line}}}. \end{cases}$$

$\boldsymbol{Y}_{C_f} = \boldsymbol{0}$ when there is no SVC in the wind power system. $\boldsymbol{Y}_{C_C} = \boldsymbol{0}$ when there is no series compensation capacitor. By simplification, the admittance model of the AC grid is

$$\Delta\boldsymbol{I}_1 = \boldsymbol{Y}\Delta\boldsymbol{U}_1 \tag{20}$$

where $\boldsymbol{Y} = \boldsymbol{Y}_{11} - \boldsymbol{Y}_{12}\boldsymbol{Y}_{22}^{-1}\boldsymbol{Y}_{21}$.

IV. STABILITY ANALYSIS AND EQUIVALENT CIRCUIT OF THE DFIG-BASED WIND POWER SYSTEM

A. EQUIVALENT POSITIVE AND NEGATIVE SEQUENCE IMPEDANCE VALUES IN THE POLAR COORDINATE SYSTEM

By the diagonalization transformation of (16), we have

$$\begin{cases} \boldsymbol{Z}_{\mathrm{R}} = \begin{bmatrix} R & 0 \\ 0 & R \end{bmatrix} \\ \boldsymbol{Z}_{L} = \boldsymbol{T} \begin{bmatrix} Z_{L+} & \\ & Z_{L-} \end{bmatrix} \boldsymbol{T}^{-1} \\ \boldsymbol{Z}_{\mathrm{C}} = \boldsymbol{T} \begin{bmatrix} Z_{C+} & \\ & Z_{C-} \end{bmatrix} \boldsymbol{T}^{-1} \end{cases} \tag{21}$$

where

$$\begin{cases} \boldsymbol{T} = \dfrac{1}{\sqrt{2}} \begin{bmatrix} 1 & 1 \\ -\mathrm{j} & \mathrm{j} \end{bmatrix} \\ \boldsymbol{T}^{-1} = \dfrac{1}{\sqrt{2}} \begin{bmatrix} 1 & \mathrm{j} \\ 1 & -\mathrm{j} \end{bmatrix} \\ Z_{L\pm} = (s \pm j\omega)L \\ Z_{C\pm} = \dfrac{1}{(s \pm j\omega)C}. \end{cases}$$

Therefore, $Z_{L\pm}$ and $Z_{C\pm}$ are the equivalent positive (negative) -sequence impedance of inductance and capacitance in the polar coordinate system.

The outgoing line can be considered a linear element, so$\boldsymbol{Y}_{11}$,$\boldsymbol{Y}_{12}$,$\boldsymbol{Y}_{21}$ and $\boldsymbol{Y}_{22}$ can be described by the capacitance, inductance and resistance. $\boldsymbol{Y}$ is given by

$$\boldsymbol{Y} = \boldsymbol{T} \begin{bmatrix} Y_{+} & \\ & Y_{-} \end{bmatrix} \boldsymbol{T}^{-1} \tag{22}$$

where Y_{+} and Y_{-} can be are the equivalent positive and negative sequence admittance values of the AC grid in the polar coordinate system.

B. STABILITY CRITERION AND EQUIVALENT CIRCUIT

The dynamic model of the DFIG-based wind farm and AC grid can be written in (23).

$$\begin{bmatrix} \Delta I \\ I\Delta\varphi \end{bmatrix} = \left(\begin{bmatrix} Y_{\mathrm{w1}}(s) & \\ & Y_{\mathrm{w4}}(s) \end{bmatrix} + \boldsymbol{Y} \right) \begin{bmatrix} \Delta U \\ U\Delta\delta \end{bmatrix} \tag{23}$$

where $Y_{\mathrm{w1}}(s) = Y_{s1}(s) + Y_{s1}(s)$ and $Y_{\mathrm{w4}}(s) = Y_{s4}(s) + Y_{s4}(s)$.

According to the equivalent equation of the DFIG-based wind power system in (23), the characteristic equation of the DFIG-based wind power system is given by

$$\left| \begin{bmatrix} Y_{\mathrm{w1}} & 0 \\ 0 & Y_{\mathrm{w4}} \end{bmatrix} + \boldsymbol{Y} \right| = 0 \tag{24}$$

where $|*|$ denotes determinant functions. Equation (24) is equivalent to

$$\left| \boldsymbol{T} \left(\begin{bmatrix} 0 & 0 \\ 0 & Y_{\mathrm{w4}} - Y_{\mathrm{w1}} \end{bmatrix} + \begin{bmatrix} Y_{\mathrm{w1}} & 0 \\ 0 & Y_{\mathrm{w1}} \end{bmatrix} + \boldsymbol{Y} \right) \boldsymbol{T}^{-1} \right| = 0. \tag{25}$$

Therefore,

$$\left| \boldsymbol{T} \left(\begin{bmatrix} 0 & 0 \\ 0 & Y_{\mathrm{w4}} - Y_{\mathrm{w1}} \end{bmatrix} \boldsymbol{T}^{-1} + \begin{bmatrix} Y_{\mathrm{w1}} + Y_{+} & 0 \\ 0 & Y_{\mathrm{w1}} + Y_{-} \end{bmatrix} \right| = 0 \tag{26}$$

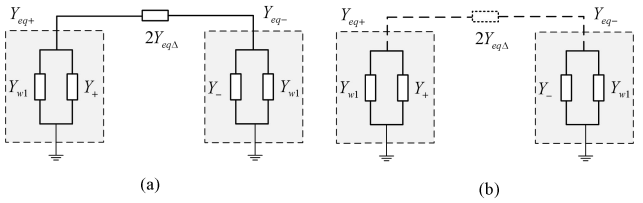

FIGURE 6. Equivalent circuit diagram of the DFIG-based wind power system (a) $Y_{\mathrm{w4}} \neq Y_{\mathrm{w1}}$; (b) $Y_{\mathrm{w4}} = Y_{\mathrm{w1}}$.

Substituting $\boldsymbol{T}$ and $\boldsymbol{T}^{-1}$ into (26), we have

$$\left| \frac{Y_{\mathrm{w4}} - Y_{\mathrm{w1}}}{2} \begin{bmatrix} 1 & -1 \\ -1 & 1 \end{bmatrix} + \begin{bmatrix} Y_{\mathrm{w1}} + Y_{+} & 0 \\ 0 & Y_{\mathrm{w1}} - Y_{-} \end{bmatrix} \right| = 0 \tag{27}$$

When $Y_{\mathrm{w4}} \neq Y_{\mathrm{w1}}$, let $Y_{eq\Delta} = Y_{\mathrm{w4}} - Y_{\mathrm{w1}}$, $Y_{eq+} = Y_{+} + Y_{\mathrm{w1}}$ and $Y_{eq-} = Y_{-} + Y_{\mathrm{w1}}$, and we have

$$\begin{aligned} &\left| \begin{bmatrix} Y_{eq+} & 0 \\ 0 & Y_{eq-} \end{bmatrix} \left(\begin{bmatrix} Y_{eq+}^{-1} & -Y_{eq-}^{-1} \\ -Y_{eq+}^{-1} & Y_{eq-}^{-1} \end{bmatrix} Y_{\mathrm{eq}\Delta} + 2\boldsymbol{I} \right) \right| = 0 \\ &\Leftrightarrow \left| \begin{bmatrix} Y_{eq+}^{-1} & -Y_{eq-}^{-1} \\ -Y_{eq+}^{-1} & Y_{eq-}^{-1} \end{bmatrix} Y_{\mathrm{eq}\Delta} + 2\boldsymbol{I} \right| = 0 \\ &\Leftrightarrow \left| \begin{bmatrix} 1 + \dfrac{Y_{\mathrm{eq}\Delta}}{2(Y_{eq+} + Y_{eq-})} & -\dfrac{Y_{\mathrm{eq}\Delta}}{2Y_{eq-}} \\ 0 & 1 \end{bmatrix} \right| = 0 \end{aligned} \tag{28}$$

Therefore, the characteristic equation of the wind power system is given by

$$1 + Y_{\mathrm{eq}\Delta} \frac{Y_{\mathrm{eq+}}^{-1} + Y_{\mathrm{eq-}}^{-1}}{2} = 0 \tag{29}$$

The characteristic equation of the wind power system corresponds to the series-parallel circuit, which is composed of the equivalent impedance of the DFIG and AC grid in the polar coordinate system. The instability of the wind power system is equivalent to the series-parallel resonance among these impedances.

Introducing the transfer function $G_{\mathrm{eq}}(s)$, we have

$$G_{\mathrm{eq}}(s) = Y_{\mathrm{eq}\Delta} \frac{Y_{\mathrm{eq+}}^{-1} + Y_{\mathrm{eq-}}^{-1}}{2} \tag{30}$$

By Nyquist's criterion, if the Nyquist curve of $G_{\mathrm{eq}}(s)$ does not surround $(-1, \mathrm{j}0)$, the wind power system is small-interference stable. Obviously, the essence of the proposed method is to simplify the special MIMO system to SISO to more simply address the stability of the system. The nonlinear problem of the eigenvalue and matrix parameters is transformed into a linear problem in the high-dimensional space.

When$Y_{\mathrm{w4}} = Y_{\mathrm{w1}}$, the stability can be determined by whether the real part of Y_{eq+} or Y_{eq-} is positive. In summary, the equivalent circuit of the DFIG-based wind power system is given as shown in Figure 6.

Introducing the total impedance of the DFIG-based wind power system asZ_{eqsum}, according to the equivalent circuit diagram in Figure 6, we have

$$Z_{\text{eqsum}} = Z_{\text{eq+}} + Z_{\text{eq}\Delta} + Z_{\text{eq-}} \tag{31}$$

According to the characteristics of series-parallel circuit, when the system loses stability, it will oscillate. The voltage-current relationship of AC grid is given by

$$\begin{bmatrix} \Delta I \\ I\Delta\varphi \end{bmatrix} = \boldsymbol{T} \begin{bmatrix} Y_+ & \\ & Y_- \end{bmatrix} \boldsymbol{T}^{-1} \begin{bmatrix} \Delta U \\ U\Delta\delta \end{bmatrix} \tag{32}$$

Furthermore, we have

$$\begin{cases} Z_+(\Delta I + jI\Delta\varphi) = \Delta U + jU\Delta\delta \\ Z_-(\Delta I - jI\Delta\varphi) = \Delta U - jU\Delta\delta \end{cases} \tag{33}$$

Through simplification, we have

$$jI\Delta\varphi = \frac{Y_+ - Y_-}{2}\Delta U + j\frac{Y_+ + Y_-}{2}U\Delta\delta \tag{34}$$

When the disturbance of the port voltage is not large, i.e., $\Delta U \approx 0$, the equation describes the dynamic relationship between the current phase angle disturbance and the voltage phase angle disturbance. Essentially, the series-parallel resonance occurs in the system equivalent circuit.

V. ANALYSIS AND SIMULATION

The stability of the DFIG-based wind power system is related to several parameters, such as the parameters of the PLL controller, AC grid parameters and wind speed. To analyze the effect of different parameters, a simulation model is established by MATLAB/SIMULINK, and the model is shown in Figure 1. The simulation sampling frequency is 5 kHz, and the simulation step size is 2 μs.

Based on previous assumptions, the DFIG has the constant power factor control strategy. The DC bus capacitor voltage is constant, and the parallel SVC is not included in the grid. The parameters of the DFIG and system are shown in Table 1 [35].

TABLE 1. Parameters of the DFIG and system.

Parameter	Value
Rated power	1.5 MW
Stator rated voltage	690 V
Rotor rated voltage	1975 V
DC bus voltage	1150 V
Stator resistance R_s	0.01 pu
Rotor resistance R_r	0.008 pu
Stator leakage inductance $L_{s\sigma}$	0.172 pu
Rotor leakage inductance $L_{r\sigma}$	0.155 pu
Magnetizing inductance L_m	2.9 pu
Integral coefficient of RSC k_{irsc}	8
Proportional coefficient of RSC k_{prsc}	0.6
Integral coefficient of PLL k_{ipll}	6
Proportional coefficient of PLL k_{ppll}	20
Outgoing line inductance L_{line}	0.23 pu

As shown in Figure 6, $Y_{eq\Delta}$ is given by

$$Y_{eq\Delta} = Y_{g4} + Y_{s4} - Y_{g1} - Y_{s1} \tag{35}$$

When the power factor is constant to 1, the impedance of the AC grid is given by

$$\begin{cases} Z_+ = (s + j\omega)L_{\text{line}} + \dfrac{1}{(s + j\omega)C_{\text{C}}} \\ Z_- = (s - j\omega)L_{\text{line}} + \dfrac{1}{(s - j\omega)C_{\text{C}}} \end{cases} \tag{36}$$

Generally, it is considered that the grid side equivalent impedance of the DFIG is much larger than the stator side equivalent resistance [26]. To simplify the analysis, the grid side circuit is considered an open circuit, and the effect of the grid side can be ignored. Therefore, substituting (35) and (36) into (30) yields the approximate open-loop transfer function $G_{\text{eq}}(s)$.

When s changes from $-j\infty$ to $+j\infty$ along the axis $j\omega$, the case where the Nyquist curve surrounds $(-1, 0)$ determines whether the system is stable and whether oscillation occurs.

A. GRID STRENGTH

The outgoing line inductance is 0.23 pu, 0.36 pu, 0.53 pu and 0.82 pu, and the Nyquist curves of the open-loop transfer function are shown in Figure 7. In addition, if the line length is changed from 0.23 pu to 0.4 pu at the time of 2.1 s, then the line length is changed from 0.4 pu to 0.8 pu at the time of 6.1 s, and the corresponding simulation waveform is shown in Figure 8.

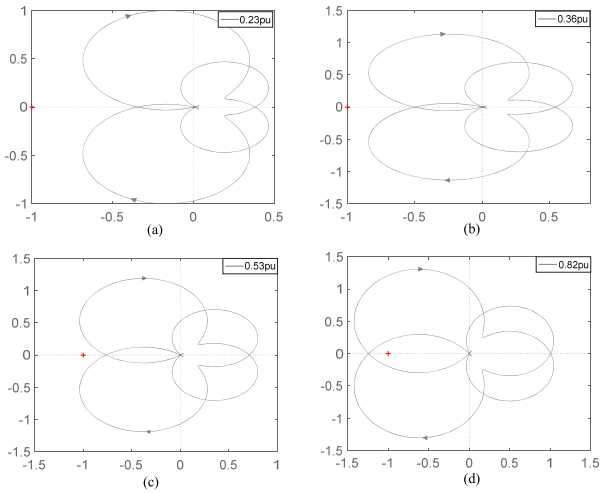

FIGURE 7. Nyquist curve of the open-loop transfer function under different line length conditions (a) L_{line} = 0.23pu; (b) L_{line} = 0.23pu; (c) L_{line} = 0.53pu; (d)L_{line} = 0.82pu.

As shown in Figure 7, when the line length is short, the point $(-1, 0)$ is outside the area enclosed by the Nyquist curve. Therefore, the system is stable, and there is no oscillation or the oscillation is convergent in this case. With the increasing length of the line, the point $(-1, 0)$ gradually

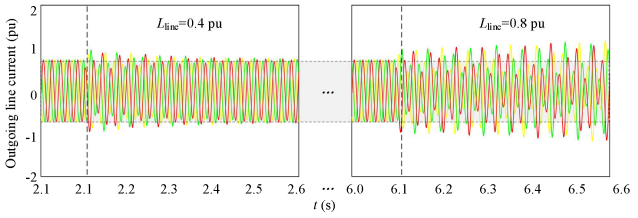

FIGURE 8. Simulation waveform of outgoing line current under different line length conditions.

approaches the Nyquist curve and is eventually enclosed within the area enclosed by the Nyquist curve. As a result, the system will oscillate and the oscillation will not converge, which is shown in Figure 8.

Thus, there is a coupling relationship between the outgoing line and the DFIG-based wind farm. In a weak grid, the oscillation and instability more likely occur in the DFIG-based wind power system.

B. WIND SPEED

The rotor speed of the DFIG is affected by the wind speed. With the increase in wind speed, the rotor speed of the DFIG also increases. The relationship between wind speed and rotor speed is shown in Table 2.

TABLE 2. Relationship between wind speed and rotor speed.

Wind speed	Rotor speed
5.5 m/s	31.25 Hz
6.5 m/s	43.62 Hz
7.5 m/s	49.95 Hz
8.5 m/s	54.73 Hz
9.5 m/s	61.42 Hz

According to the DFIG parameters in Table 1, the Nyquist curve of the open-loop transfer function at different wind speeds is shown in Figure 9. In addition, the impedance of the wind power system at different wind speeds is shown in Figure 10.

As shown in Figure 10, regardless of the sub-synchronous or super-synchronous rotor speed, the intersection of the Nyquist curve on the real axis moves to the right side and is continuously away from the point $(-1, 0)$ with the increase in wind speed. Thus, for a greater wind speed, the DFIG-based wind power system is less likely unstable. Figure 10 shows that the damping of the wind power system increases with the increase in wind speed, so it is more possible to oscillate at low wind speeds.

C. PI PARAMETERS OF THE PLL CONTROLLER

By changing the proportional and integral coefficients of PLL, the effects of the PLL parameters on the stability and oscillation characteristics of the DFIG-based wind power system are studied. Considering the oscillation frequency range of 18.4-18.6 Hz during oscillation, the equivalent impedance

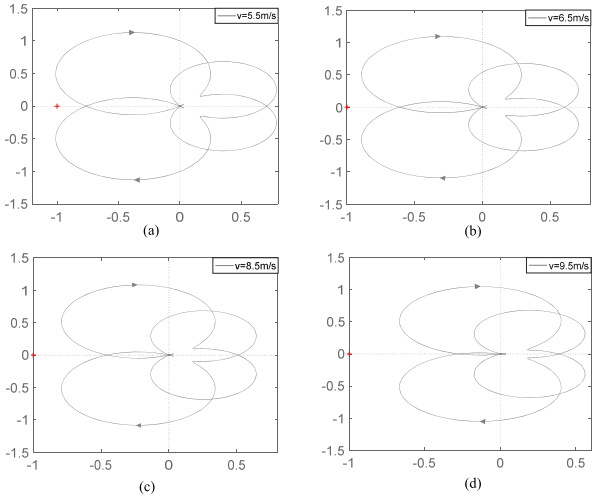

FIGURE 9. Nyquist curve of the open-loop transfer function at different wind speeds (a) v =5.5m/s; (b) v =6.5m/s; (c) v =8.5m/s; (d) v =9.5m/s.

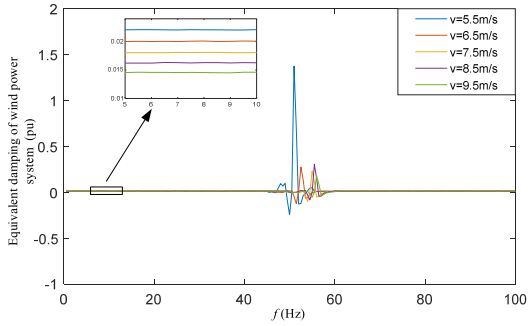

FIGURE 10. Impedance of the wind power system at different wind speeds.

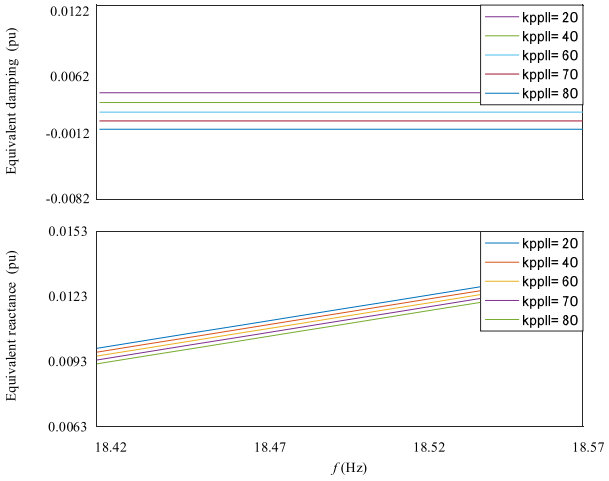

FIGURE 11. Effect of $k_{p\text{pll}}$ on the DFIG-based wind power system equivalent impedance.

of the DFIG-based wind power system in this frequency range is analyzed. The effects of the proportional and integral coefficients of PLL on the equivalent impedance are shown in Figure 11 and Figure 12, respectively.

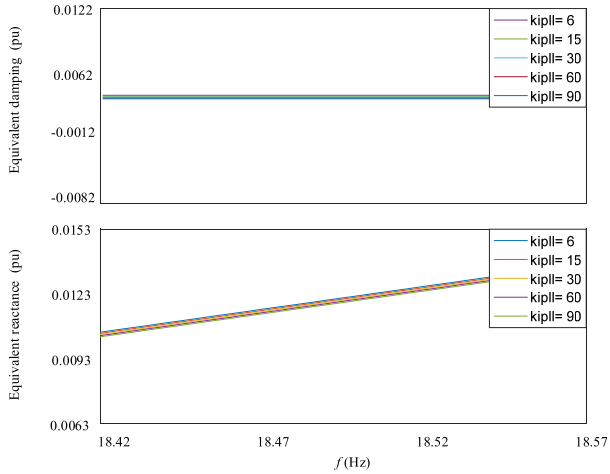

FIGURE 12. Effect of $k_{i\text{pll}}$ on the DFIG-based wind power system equivalent impedance.

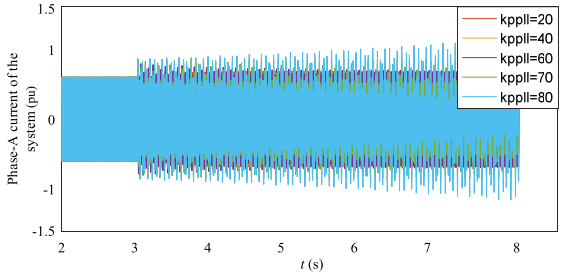

FIGURE 13. Phase-A current waveforms of the system for different $k_{p\text{pll}}$.

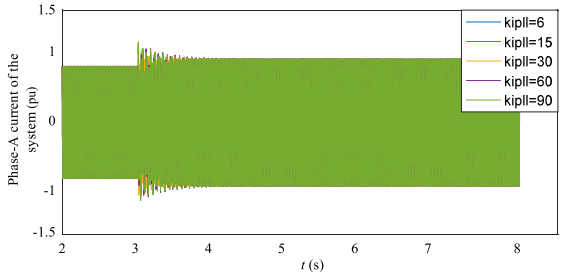

FIGURE 14. Phase-A current waveforms of the system for different $k_{i\text{pll}}$.

As shown in Figures 11 and 12, the equivalent resistance of the system decreases with the increase in $k_{p\text{pll}}$, which makes the stability of the system worse and easier to oscillate. When $k_{p\text{pll}} < 60$, the oscillation of the system is also attenuated. However, when $k_{p\text{pll}} > 75$, the system oscillates and is divergent. Unlike the proportional coefficient, the integral coefficient $k_{i\text{pll}}$ has little influence on the system stability. Even if $k_{i\text{pll}}$ is increased several times, the system damping remains positive, and the system remains stable.

The simulation of the DFIG-based wind power system under different PLL parameters is shown in Figure 13 and Figure 14.

As shown in Figures 13 and 14, the oscillation of the system gradually diverges from convergence with the increase in $k_{p\text{pll}}$, whereas the convergence tendency of the system oscillation does not change, and the convergence speed does not significantly change with the increase in $k_{i\text{pll}}$. Therefore, the PLL integral coefficient has little influence on the system oscillation, while the proportional coefficient greatly affects the system oscillation.

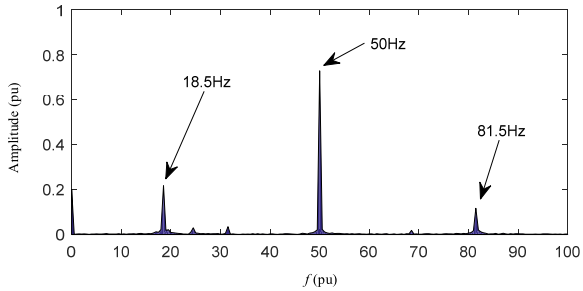

FIGURE 15. FFT analysis of the current waveform.

For $k_{p\text{pll}} = 75$, the oscillating current waveform is analyzed by FFT, and the FFT analysis results are shown in Figure 15.

When the system oscillates, there are obvious harmonic components of 18.5 Hz and 81.5 Hz, which shows that the DFIG-based wind power system is coupled between frequencies. The traditional positive and negative sequence component analysis method are based on a single frequency component, causing errors when ignoring the frequency coupling. The proposed method can avoid this problem effectively, and the analysis results will be more accurate.

VI. CONCLUSION

The impedance model of the DFIG-based wind power system in the polar coordinate system is established by using the small-signal analysis method, and the equivalent impedance analysis circuit considering frequency coupling is provided in this paper. Furthermore, the stability and oscillation mechanism of the system are revealed based on Nyquist criterion. The main conclusions are as follows:

The AC grid strength has an important effect on the stability of the DFIG-based wind power system, and it is more likely to lose stability and oscillate in the weak AC grid.

The change in wind speed makes the DFIG equivalent impedance have time-varying characteristics, which affects the stability of the wind power system. The stability of the system increases with the increase in wind speed, and it is more likely to lose stability at low wind speeds.

The increase in the PLL proportional coefficient will reduce the system damping and decrease the system stability. The effect of the PLL integral coefficient on the system damping and stability is negligible.

In addition, the DFIG controller parameters, location of the static var compensator(SVC), and serial compensation of the outgoing line also affect the stability and oscillation of the wind power system. Therefore, further research should be conducted in the future.

VII. APPENDIX

A. DETAILED DERIVATION PROCESS OF THE DFIG DYNAMIC MODEL

Assume that the inner loop output voltage and PWM modulation voltage are equal, and the outer loop output is constant. Therefore, we have $\Delta U_{rd}^* = \Delta U_{rd}$, $\Delta U_{rq}^* = \Delta U_{rq}$, $\Delta U_{gd}^* = \Delta U_{gd}$ and $\Delta U_{gq}^* = \Delta U_{gq}$.

1) ADMITTANCE MODELING OF THE DFIG REGARDLESS OF THE OUTER LOOP CONTROL

Linearize (2) and the dynamic equation of the PLL in the corresponding polar coordinates is given

$$\begin{cases} \Delta\theta_{\text{pll}} = G_{\text{pll}}(s)\Delta U_q = G_{\text{pll}}(s)U\Delta\theta_U \\ \Delta\omega = s\Delta\theta_{\text{pll}} \end{cases} \tag{A1}$$

According to Figure 1, we have

$$\begin{cases} \Delta\theta_{\text{U}} = \Delta\delta - \Delta\theta_{\text{pll}} \\ \Delta\theta_{\text{I}} = \Delta\varphi - \Delta\theta_{\text{pll}} \end{cases} \tag{A2}$$

With simultaneous (B1) and (B2), we have

$$\Delta\theta_{\text{pll}} = \frac{G_{\text{pll}}(s)U}{1 + G_{\text{pll}}(s)U}\Delta\delta \tag{A3}$$

Linearizing (3)-(7) yields

$$\begin{bmatrix} \Delta U_{rd}^* \\ \Delta U_{rq}^* \end{bmatrix} = G_{\text{rsc}}(s)\begin{bmatrix} \Delta I_{rd}^* \\ \Delta I_{rq}^* \end{bmatrix} - \begin{bmatrix} G_{\text{rsc}}(s) & -\omega_2 L_{rr} \\ \omega_2 L_{rr} & G_{\text{rsc}}(s) \end{bmatrix}\begin{bmatrix} \Delta I_{rd} \\ \Delta I_{rq} \end{bmatrix} \tag{A4}$$

$$\begin{bmatrix} \Delta U_{gd}^* \\ \Delta U_{gq}^* \end{bmatrix} = G_{\text{gsc}}(s)\begin{bmatrix} \Delta I_{gd}^* \\ \Delta I_{gq}^* \end{bmatrix} - \begin{bmatrix} G_{\text{gsc}}(s) & -\omega_1 L_g \\ \omega_1 L_g & G_{\text{gsc}}(s) \end{bmatrix}\begin{bmatrix} \Delta I_{gd} \\ \Delta I_{gq} \end{bmatrix} \tag{A5}$$

$$\begin{bmatrix} \Delta U_{sd} \\ \Delta U_{sq} \end{bmatrix} = \begin{bmatrix} R_s + sL_s & -\omega_1 L_s \\ \omega_1 L_s & R_s + sL_s \end{bmatrix}\begin{bmatrix} \Delta I_{sd} \\ \Delta I_{sq} \end{bmatrix} + \begin{bmatrix} sL_m & -\omega_1 L_m \\ \omega_1 L_m & sL_m \end{bmatrix}\begin{bmatrix} \Delta I_{rd} \\ \Delta I_{rq} \end{bmatrix} \tag{A6}$$

$$\begin{bmatrix} \Delta U_{rd} \\ \Delta U_{rq} \end{bmatrix} = \begin{bmatrix} R_r + sL_r & -\omega_2 L_r \\ \omega_2 L_r & R_r + sL_r \end{bmatrix}\begin{bmatrix} \Delta I_{rd} \\ \Delta I_{rq} \end{bmatrix} + \begin{bmatrix} sL_m & -\omega_2 L_m \\ \omega_2 L_m & sL_m \end{bmatrix}\begin{bmatrix} \Delta I_{sd} \\ \Delta I_{sq} \end{bmatrix} \tag{A7}$$

$$\begin{bmatrix} \Delta U_{sd} \\ \Delta U_{sq} \end{bmatrix} = \begin{bmatrix} R_g + sL_g & -\omega_1 L_g \\ \omega_1 L_g & R_g + sL_g \end{bmatrix}\begin{bmatrix} \Delta I_{gd} \\ \Delta I_{gq} \end{bmatrix} + \begin{bmatrix} \Delta U_{gd}^* \\ \Delta U_{gq}^* \end{bmatrix} \tag{A8}$$

With simultaneous (B4) and (B7), we obtain

$$G_{\text{rsc}}(s)\begin{bmatrix} \Delta I_{rd}^* \\ \Delta I_{rq}^* \end{bmatrix} = L_m\begin{bmatrix} s & -\omega_2 \\ \omega_2 & s \end{bmatrix}\begin{bmatrix} \Delta I_{sd} \\ \Delta I_{sq} \end{bmatrix} + \boldsymbol{Z}_{\text{rsc}}\begin{bmatrix} \Delta I_{rd} \\ \Delta I_{rq} \end{bmatrix} \tag{A9}$$

where $\boldsymbol{Z}_{\text{rsc}} = \begin{bmatrix} G_{\text{rsc}}(s) & \omega_2 L_m \\ -\omega_2 L_m & G_{\text{rsc}}(s) \end{bmatrix}$.

Since the dynamics of the outer-loop controller are ignored, the following equation holds.

$$\begin{bmatrix} \Delta I_{rd}^* \\ \Delta I_{rq}^* \end{bmatrix} = 0, \quad \begin{bmatrix} \Delta I_{gd}^* \\ \Delta I_{gq}^* \end{bmatrix} = 0 \tag{A10}$$

Substituting (B9) and (B10) into (B6) yields

$$\begin{bmatrix} \Delta U_{sd} \\ \Delta U_{sq} \end{bmatrix} = \begin{bmatrix} R_s + sL_s & -\omega_1 L_s \\ \omega_1 L_s & R_s + sL_s \end{bmatrix}\begin{bmatrix} \Delta I_{sd} \\ \Delta I_{sq} \end{bmatrix} + L_m^2\begin{bmatrix} s & -\omega_1 \\ \omega_1 & s \end{bmatrix}\boldsymbol{Z}_{\text{rsc}}^{-1}\begin{bmatrix} s & -\omega_2 \\ \omega_2 & s \end{bmatrix}\begin{bmatrix} \Delta I_{sd} \\ \Delta I_{sq} \end{bmatrix} \tag{A11}$$

Generally, the stator resistance of the DFIG is small and negligible. In addition, $L_m \gg L_{s\sigma}$ and $L_m \gg L_{r\sigma}$; by simplification, we have

$$\begin{bmatrix} \Delta U_{sd} \\ \Delta U_{sq} \end{bmatrix} = \begin{bmatrix} Z_{s1} & Z_{s2} \\ Z_{s3} & Z_{s4} \end{bmatrix}\begin{bmatrix} \Delta I_{sd} \\ \Delta I_{sq} \end{bmatrix} \tag{A12}$$

where

$$\begin{cases} Z_{s1} = sL_{\sigma s} + \dfrac{\omega_1 R_r}{\omega_2} + sL_{\sigma r} - \dfrac{\omega_1}{\omega_2}G_{\text{rsc}}(s) \\ Z_{s2} = -\omega_1 L_{\sigma s}^2/L_s \\ Z_{s3} = \omega_1 L_{\sigma s}^2/L_s \\ Z_{s4} = sL_{\sigma s} + \dfrac{\omega_1 R_r}{\omega_2} + sL_{\sigma r} - \dfrac{\omega_1}{\omega_2}G_{\text{rsc}}(s). \end{cases}$$

If we ignore the GSC equivalent impedance in the analysis, transform (A12) into the polar coordinate expression and substitute (A2) and (A3) into (A12), we have the relationship between current and voltage in polar coordinates, as shown in (A13).

$$\begin{bmatrix} \Delta I_s \\ I_s\Delta\varphi \end{bmatrix} = \begin{bmatrix} Y_{s1} & Y_{s2} \\ Y_{s3} & Y_{r4} \end{bmatrix}\begin{bmatrix} \Delta U_s \\ U_s\Delta\delta \end{bmatrix} \tag{A13}$$

where

$$\begin{cases} Y_{s1} = \dfrac{Z_{s4}}{Z_{s1}Z_{s4} - Z_{s2}Z_{s3}}\cos\theta_{\text{I}} + \dfrac{Z_{s3}}{Z_{s1}Z_{s4} - Z_{s2}Z_{s3}}\sin\theta_{\text{I}} \\ Y_{s2} = -\dfrac{Z_{s4}}{Z_{s1}Z_{s4} - Z_{s2}Z_{s3}}\sin\theta_{\text{I}} + \dfrac{Z_{s3}}{Z_{s1}Z_{s4} - Z_{s2}Z_{s3}}\cos\theta_{\text{I}} \\ Y_{s3} = \dfrac{1}{1 + G_{\text{pll}}(s)U_s}\left(\dfrac{Z_{s2}}{Z_{s1}Z_{s4} - Z_{s2}Z_{s3}}\cos\theta_{\text{I}} + \dfrac{Z_{s1}}{Z_{s1}Z_{s4} - Z_{s2}Z_{s3}}\sin\theta_{\text{I}}\right) \\ Y_{s4} = \dfrac{1}{1 + G_{\text{pll}}(s)U_s}\left(-\dfrac{Z_{s2}}{Z_{s1}Z_{s4} - Z_{s2}Z_{s3}}\sin\theta_{\text{I}} + \dfrac{Z_{s1}}{Z_{s1}Z_{s4} - Z_{s2}Z_{s3}}\cos\theta_{\text{I}}\right) \end{cases}$$

Furthermore, according to the assumption that the output power factor of the DFIG is 1, $\cos\theta_{\text{I}} \approx 1$, and $\sin\theta_{\text{I}} \approx 0$. Thus, we have

$$\begin{cases} Y_{s1} = \dfrac{1}{\frac{R_r}{\sigma_{slip}} + sL_{\sigma s} + sL_{\sigma r} - \frac{1}{\sigma_{slip}}G_{\text{rsc}}(s)} \\ Y_{s2} = 0 \\ Y_{s3} = 0 \\ Y_{s4} = \dfrac{1}{(1 + G_{\text{pll}}(s)U_s)(\frac{R_r}{\sigma_{slip}} + sL_{\sigma s} + sL_{\sigma r} - \frac{1}{\sigma_{slip}}G_{\text{rsc}}(s))} \end{cases} \tag{A14}$$

Similarly, the GSC equivalent impedance can be obtained according to (B5)-(B8), as shown in (A15).

$$\begin{bmatrix} \Delta U_{sd} \\ \Delta U_{sq} \end{bmatrix} = \begin{bmatrix} Z_{g1} & Z_{g2} \\ Z_{g3} & Z_{g4} \end{bmatrix} \begin{bmatrix} \Delta I_{gd} \\ \Delta I_{gq} \end{bmatrix} \tag{A15}$$

where

$$\begin{cases} Z_{g1} = R_g + sL_g - G_{\mathrm{gsc}}(s) \\ Z_{g2} = 0 \\ Z_{g3} = 0 \\ Z_{g4} = R_g + sL_g - G_{\mathrm{gsc}}(s). \end{cases}$$

Transforming (A15) into a polar coordinate expression, substituting (A2) and (A3) into (A15), and ignoring the resistance of the filter, we have the relationship between the current and the voltage in the polar coordinate system, as shown in (A16).

$$\begin{bmatrix} \Delta I_g \\ I_g \Delta\varphi \end{bmatrix} = \begin{bmatrix} Y_{g1} & Y_{g2} \\ Y_{g3} & Y_{g4} \end{bmatrix} \begin{bmatrix} \Delta U_s \\ U_s \Delta\delta \end{bmatrix} \tag{A16}$$

where

$$\begin{cases} Y_{g1} = \dfrac{1}{sL_g - G_{\mathrm{gsc}}(s)} \\ Y_{g2} = 0 \\ Y_{g3} = 0 \\ Y_{g4} = \dfrac{1}{(1 + G_{\mathrm{pll}}(s)U_s)(sL_g - G_{\mathrm{gsc}}(s))}. \end{cases}$$

2) CONSIDERING THE PQ CONTROL OF THE RSC

According to the PQ control block in Figure 3, we have

$$\begin{bmatrix} \Delta I_{rd}^* \\ \Delta I_{rq}^* \end{bmatrix} = G_{\mathrm{pq}}(s) \begin{bmatrix} \Delta P \\ \Delta Q \end{bmatrix} \tag{A17}$$

Substituting (A17) into (A4) yields

$$\begin{bmatrix} \Delta U_{rd}^* \\ \Delta U_{rq}^* \end{bmatrix} = G_{\mathrm{rsc}}(s)G_{\mathrm{pq}}(s) \begin{bmatrix} \Delta P \\ \Delta Q \end{bmatrix} - \begin{bmatrix} G_{\mathrm{rsc}}(s) & -\omega_2 L_{rr} \\ \omega_2 L_{rr} & G_{\mathrm{rsc}}(s) \end{bmatrix} \begin{bmatrix} \Delta I_{rd} \\ \Delta I_{rq} \end{bmatrix} \tag{A18}$$

Linearizing equation (7), we have

$$\begin{bmatrix} \Delta P \\ \Delta Q \end{bmatrix} = \begin{bmatrix} U_{sd} & \\ & U_{sq} \end{bmatrix} \begin{bmatrix} \Delta I_{sd} \\ \Delta I_{sq} \end{bmatrix} + \begin{bmatrix} I_{sd} & \\ & I_{sq} \end{bmatrix} \begin{bmatrix} \Delta U_{sd} \\ \Delta U_{sq} \end{bmatrix} \tag{A19}$$

Substituting (A19) into (A18) yields the relationship between the stator side current and the voltage, as shown in (A20).

$$\begin{bmatrix} \Delta U_{sd} \\ \Delta U_{sq} \end{bmatrix} = \begin{bmatrix} Z_{s1} & Z_{s2} \\ Z_{s3} & Z_{s4} \end{bmatrix} \begin{bmatrix} \Delta I_{sd} \\ \Delta I_{sq} \end{bmatrix} \tag{A20}$$

where

$$\begin{cases} Z_{s1} = \dfrac{sL_{\sigma s} + \frac{R_r}{\sigma_{slip}} + sL_{\sigma r} + G_{\mathrm{rsc}}(s)G_{\mathrm{pq}}(s)U_s - \frac{1}{\sigma_{slip}}G_{\mathrm{rsc}}(s)}{1 - \frac{1}{\sigma_{slip}}G_{\mathrm{rsc}}(s)G_{\mathrm{pq}}(s)I_s} \\ Z_{s2} = -\dfrac{\omega_1 L_{\sigma s}^2 / L_s}{1 - \frac{1}{\sigma_{slip}}G_{\mathrm{rsc}}(s)G_{\mathrm{pq}}(s)I_s} \\ Z_{s3} = \dfrac{\omega_1 L_{\sigma s}^2 / L_s}{1 - \frac{1}{\sigma_{slip}}G_{\mathrm{rsc}}(s)G_{\mathrm{pq}}(s)I_s} \\ Z_{s4} = \dfrac{sL_{\sigma s} + \frac{R_r}{\sigma_{slip}} + sL_{\sigma r} + G_{\mathrm{rsc}}(s)G_{\mathrm{pq}}(s)U_s - \frac{1}{\sigma_{slip}}G_{\mathrm{rsc}}(s)}{1 - \frac{1}{\sigma_{slip}}G_{\mathrm{rsc}}(s)G_{\mathrm{pq}}(s)I_s}. \end{cases}$$

Substituting (A1), (A2) and (A3) into (A20) yields the approximate dynamic model of the DFIG in the polar coordinate, as shown in (B21).

$$\begin{bmatrix} \Delta I_s \\ I_s \Delta\varphi \end{bmatrix} = \begin{bmatrix} Y_{s1} & Y_{s2} \\ Y_{s3} & Y_{r4} \end{bmatrix} \begin{bmatrix} \Delta U_s \\ U_s \Delta\delta \end{bmatrix} \tag{A21}$$

where

$$\begin{cases} Y_{s1} = \dfrac{1}{sL_{\sigma s} + \frac{R_r}{\sigma_{slip}} + sL_{\sigma r} + G_{\mathrm{rsc}}(s)G_{\mathrm{pq}}(s)U_s - \frac{1}{\sigma_{slip}}G_{\mathrm{rsc}}(s)} \\ Y_{s2} = 0 \\ Y_{s3} = 0 \\ Y_{s4} = \dfrac{\frac{1}{1+G_{\mathrm{pll}}(s)U_s}}{sL_{\sigma s} + \frac{R_r}{\sigma_{slip}} + sL_{\sigma r} + G_{\mathrm{rsc}}(s)G_{\mathrm{pq}}(s)U_s - \frac{1}{\sigma_{slip}}G_{\mathrm{rsc}}(s)}, \end{cases}$$

3) CONSIDERING DC BUS VOLTAGE CONTROL

Linearizing equations (13) and (14), we have

$$\begin{bmatrix} \Delta I_{gd}^* \\ \Delta I_{gq}^* \end{bmatrix} = G_{\mathrm{dc}}(s) \begin{bmatrix} \Delta U_{\mathrm{dc}} \\ 0 \end{bmatrix} \tag{A22}$$

$$\begin{aligned} sU_{\mathrm{dc0}}\Delta U_{\mathrm{dc}}C_{\mathrm{dc}} &= -\frac{1 - \sigma_{slip}}{\sigma_{slip}}\Delta P_{\mathrm{g}} \\ &\approx \frac{\sigma_{slip} - 1}{\sigma_{slip}}(U_{s0}\Delta I_{gd} + I_{g0}\Delta U_{sd}) \end{aligned} \tag{A23}$$

Substituting (A23) into (A22) yields

$$\begin{bmatrix} \Delta I_{gd}^* \\ \Delta I_{gq}^* \end{bmatrix} = \frac{G_{\mathrm{dc}}(s)U_{s0}(\sigma_{slip} - 1)}{sU_{\mathrm{dc0}}C_{\mathrm{dc}}\sigma_{slip}} \begin{bmatrix} \Delta I_{gd} \\ 0 \end{bmatrix} + \frac{G_{\mathrm{dc}}(s)I_{g0}(\sigma_{slip} - 1)}{sU_{\mathrm{dc0}}C_{\mathrm{dc}}\sigma_{slip}} \begin{bmatrix} \Delta U_{gd} \\ 0 \end{bmatrix} \tag{A24}$$

Substituting (A1)-(A3) into (A5), (A8) and (A24) yields the GSC dynamic model in the polar coordinate, as written in (A25).

$$\begin{bmatrix} \Delta I_g \\ I_g \Delta\varphi \end{bmatrix} = \begin{bmatrix} Y_{g1} & Y_{g2} \\ Y_{g3} & Y_{g4} \end{bmatrix} \begin{bmatrix} \Delta U_s \\ U_s \Delta\delta \end{bmatrix} \tag{A25}$$

where

$$\begin{cases} Y_{g1} = \dfrac{1 - \frac{G_{\rm gsc}(s)G_{\rm dc}(s)I_{s0}(\sigma_{slip}-1)}{\sigma_{slip}sU_{\rm dc0}C_{\rm dc}}}{sL_g - G_{gsc}(s)(1 - \frac{G_{\rm dc}(s)U_{s0}(\sigma_{slip}-1)}{\sigma_{slip}sU_{\rm dc0}C_{\rm dc}})} \\ Y_{g2} = 0 \\ Y_{g3} = 0 \\ Y_{g4} = \dfrac{1}{(1 + G_{\rm pll}(s)U_s)(sL_g - G_{\rm gsc}(s))}. \end{cases}$$

ACKNOWLEDGMENT

Wei Jin would like to thank his respectable teacher Prof. Yuping Lu for his time and guidance.

REFERENCES

[1] V. Telukunta, J. Pradhan, A. Agrawal, M. Singh, and S. G. Srivani, "Protection challenges under bulk penetration of renewable energy resources in power systems: A review," *CSEE J. Power Energy Syst.*, vol. 3, no. 4, pp. 365–379, Dec. 2017.

[2] A. A. van der Meer, M. Ndreko, M. Gibescu, and M. A. M. M. van der Meijden, "The effect of FRT behavior of VSC-HVDC-connected offshore wind power plants on AC/DC system dynamics," *IEEE Trans. Power Del.*, vol. 31, no. 2, pp. 878–887, Apr. 2016.

[3] A. Haddadi, I. Kocar, U. Karaagac, H. Gras, and E. Farantatos, "Impact of wind generation on power swing protection," *IEEE Trans. Power Del.*, vol. 34, no. 3, pp. 1118–1128, Jun. 2019.

[4] W. Jin, Y. Lu, and T. Huang, "Study on non-fundamental frequency components in the output current of DFIG-based wind turbines during faults," in *Proc. China Int. Conf. Electr. Distrib. (CICED)*, Tianjin, China, Sep. 2018, pp. 1638–1644.

[5] M. Nagpal and C. Henville, "Impact of power-electronic sources on transmission line ground fault protection," *IEEE Trans. Power Del.*, vol. 33, no. 1, pp. 62–70, Feb. 2018.

[6] W. Liu, X. Xie, J. Huang, C. Zhang, and C. Yin, "Frequency-coupled impedance model and stability analysis of grid-connected converter," *Automat. Electr. Power Syst.*, vol. 43, no. 3, pp. 138–146, Feb. 2019.

[7] M. Céspedes and J. Sun, "Impedance shaping of three-phase grid-parallel voltage-source converters," in *Proc. 27th Annu. IEEE Appl. Power Electron. Conf. Expo. (APEC)*, Orlando, Orlando, FL, USA, Feb. 2012, pp. 754–760.

[8] X. L. Dong, X. R. Xie, Y. D. Han, and J. Li, "Mechanism study of DFIG-related SSR based on separate stator and rotor torque analysis," *Proc. CSEE*, vol. 35, no. 19, pp. 4861–4869, Jun. 2015.

[9] C. Liu, X. Tian, K. Chen, Y. Su, and Y. Li, "Effect of PLL on transient performance of wind turbines generator under voltage phase jump," *J. Eng.*, vol. 2019, no. 16, pp. 967–971, Apr. 2019.

[10] S. Shah and L. Parsa, "Impedance modeling of three-phase voltage source converters in DQ, sequence, and phasor domains," *IEEE Trans. Energy Convers.*, vol. 32, no. 3, pp. 1139–1150, Sep. 2017.

[11] B. Wen, D. Boroyevich, R. Burgos, P. Mattavelli, and Z. Shen, "Small-signal stability analysis of three-phase AC systems in the presence of constant power loads based on measured $d-q$ frame impedances," *IEEE Trans. Power Electron.*, vol. 30, no. 10, pp. 5952–5963, Oct. 2015.

[12] X. Wang, L. Harnefors, and F. Blaabjerg, "Unified impedance model of grid-connected voltage-source converters," *IEEE Trans. Power Electron.*, vol. 33, no. 2, pp. 1775–1787, Feb. 2018.

[13] M. Céspedes and J. Sun, "Modeling and mitigation of harmonic resonance between wind turbines and the grid," in *Proc. IEEE Energy Convers. Congr. Expo.*, Phoenix, AZ, USA, Sep. 2011, pp. 2109–2116.

[14] J. Sun, Z. Bing, and K. J. Karimi, "Input impedance modeling of multipulse rectifiers by harmonic linearization," *IEEE Trans. Power Electron.*, vol. 24, no. 12, pp. 2812–2820, Dec. 2009.

[15] Y. Wang, X. Chen, and J. Chen, "Analysis of positive-sequence and negative-sequence impedance modeling of three-phase LCL-type grid-connected inverters based on harmonic linearization," *Proc. CSEE*, vol. 36, no. 21, pp. 5890–5898, Mar. 2016.

[16] M. Cespedes and J. Sun, "Impedance modeling and analysis of grid-connected voltage-source converters," *IEEE Trans. Power Electron.*, vol. 29, no. 3, pp. 1254–1261, Mar. 2014.

[17] M. K. Bakhshizadeh, X. Wang, F. Blaabjerg, J. Hjerrild, Ł. Kocewiak, C. L. Bak, and B. Hesselbæk, "Couplings in phase domain impedance modeling of grid-connected converters," *IEEE Trans. Power Electron*, vol. 31, no. 10, pp. 6792–6796, Oct. 2016.

[18] Z. Miao, "Impedance-model-based SSR analysis for type 3 wind generator and series-compensated network," *IEEE Trans. Energy Convers.*, vol. 27, no. 4, pp. 984–991, Dec. 2012.

[19] L. Piyasinghe, Z. Miao, J. Khazaei, and L. Fan, "Impedance model-based SSR analysis for TCSC compensated type-3 wind energy delivery systems," *IEEE Trans. Sustain. Energy*, vol. 6, no. 1, pp. 179–187, Jan. 2015.

[20] X. Dong, X. R. Xie, J. Li, and Y. D. Han, "Comparative study of the impact on subsynchronous resonance characteristics from the different location of wind generators in a large wind farm," *Proc. CSEE*, vol. 35, no. 20, pp. 5173–5180, Jun. 2015.

[21] K. Y. Liao, S. Tao, and L. T. Yao, "Study on frequency-domain modeling and time-varying characteristics of DFIG input impedance with excitation under static reference frame," *Proc. CSEE*, vol. 38, no. 16, pp. 4886–4897, Jan. 2018.

[22] D. Zhang, Y. Wang, J. Hu, S. Ma, Q. He, and Q. Guo, "Impacts of PLL on the DFIG-based WTG's electromechanical response under transient conditions: Analysis and modeling," *CSEE J. Power Energy Syst.*, vol. 2, no. 2, pp. 30–39, Jun. 2016.

[23] X. Xi, H. Geng, and G. Yang, "Enhanced model of the doubly fed induction generator-based wind farm for small-signal stability studies of weak power system," *IET Renew. Power Gener.*, vol. 8, no. 7, pp. 765–774, Sep. 2014.

[24] L. Fan and Z. Miao, "Nyquist-stability-criterion-based SSR explanation for type-3 wind generators," *IEEE Trans. Energy Convers.*, vol. 27, no. 3, pp. 807–809, Sep. 2012.

[25] J. Hu, B. Wang, W. Wang, H. Tang, Y. Chi, and Q. Hu, "Small signal dynamics of DFIG-based wind turbines during riding through symmetrical faults in weak AC grid," *IEEE Trans. Energy Convers.*, vol. 32, no. 2, pp. 720–730, Jun. 2017.

[26] H. H. Xin, Z. H. Li, and W. Dong, "Generalized-impedance and stability criterion for grid-connected converters," *Proc. CSEE*, vol. 37, no. 5, pp. 1277–1293, Mar. 2017.

[27] C. Zhu, L. Fan, and M. Hu, "Control and analysis of DFIG-based wind turbines in a series compensated network for SSR damping," in *Proc. IEEE PES Gen. Meeting*, Providence, RI, USA, Jul. 2010, pp. 1–6.

[28] Y. Li, H. Liu, M. Yin, and W. Song, "SSR analysis of DFIG-based series-compensated system based on complex torque analysis method," in *Proc. Int. Conf. Power Syst. Technol. (POWERCON)*, Guangzhou, China, Nov. 2018, pp. 1903–1908.

[29] I. Setiawan, M. Facta, A. Priyadi, and M. H. Purnomo, "Comparison of three popular PLL schemes under balanced and unbalanced grid voltage conditions," in *Proc. 8th Int. Conf. Inf. Technol. Elect. Eng. (ICITEE)*, Yogyakarta, Indonesia, Oct. 2016, pp. 1–6.

[30] J. Ma, Y. Qiu, Y. Li, W. Zhang, Z. Song, and J. S. Thorp, "Research on the impact of DFIG virtual inertia control on power system small-signal stability considering the phase-locked loop," *IEEE Trans. Power Syst.*, vol. 32, no. 3, pp. 2094–2105, May 2017.

[31] W. Jin, Y. Lu, L. Zhu, and C. Tang, "Research on mechanism of large-scale wind turbines off-grid and preventive relay protection strategy," in *Proc. China Int. Conf. Electr. Distrib. (CICED)*, Xi'an, China, Aug. 2016, pp. 1–5.

[32] U. Karaagac, S. O. Faried, J. Mahseredjian, and A.-A. Edris, "Coordinated control of wind energy conversion systems for mitigating subsynchronous interaction in DFIG-based wind farms," *IEEE Trans. Smart Grid*, vol. 5, no. 5, pp. 2440–2449, Sep. 2014.

[33] J. Yao, X. Wang, J. Li, R. Liu, and H. Zhang, "Sub-synchronous resonance damping control for series-compensated DFIG-based wind farm with improved particle swarm optimization algorithm," *IEEE Trans. Energy Convers.*, vol. 34, no. 2, pp. 849–859, Jun. 2019.

[34] C. Tang, Y. P. Lu, and T. Huang, "Analysis on transient equivalent circuit of doubly fed induction generator with crowbar protection," in *Proc. 2nd Int. Conf. Power Renew. Energy (ICPRE)*, Chengdu, China, Sep. 2017, pp. 208–213.

[35] W. Jin, Y. P. Lu, and T. Huang, "Improved blocking scheme for CPL current protection in wind farms using the amplitude ratio and phase difference," *IEEE Access*, vol. 7, pp. 2169–3536, 2019.

WEI JIN was born in Xuzhou, China, in 1987. He received the B.E. degree from Hohai University, Nanjing, China, in 2011, and the M.E. degree from the China University of Mining and Technology, Xuzhou, China, in 2013. He is currently pursuing the Ph.D. degree with Southeast University, Nanjing. His current research interests include power system protection and control in distribution systems with DGs.

YUPING LU was born in Danyang, China, in 1962. He received the Ph.D. degree in electrical engineering from City University, U.K., in 2003.

He is currently a Professor with the Southeast University of China. His research interests include power system protection, especially digital relaying of generator-transformer units, and protection and control techniques in distribution systems with DGs. He severs as a Reviewer for the *International Journal of Power and Energy Systems* and the IEEE PES Transactions on Power Delivery, and a member of the Technical Committee on Intelligent Power and Energy System.